

Discrimination of thermal baths by single qubit probes

Ilaria Gianani,^{1,2} Donato Farina,^{3,4} Marco Barbieri,^{1,5} Valeria Cimini,¹ Vasco Cavina,⁶ and Vittorio Giovannetti⁷

¹*Dipartimento di Scienze, Università degli Studi Roma Tre, Via della Vasca Navale 84, 00146 Rome, Italy*

²*Dipartimento di Fisica, Sapienza Università di Roma, Piazzale Aldo Moro 5, 00185 Rome, Italy*

³*NEST, Scuola Normale Superiore, I-56126 Pisa, Italy*

⁴*Istituto Italiano di Tecnologia, Graphene Labs, Via Morego 30, I-16163 Genova, Italy*

⁵*Istituto Nazionale di Ottica - CNR, Largo Enrico Fermi 6, 50125 Firenze, Italy*

⁶*Complex Systems and Statistical Mechanics, Physics and Materials*

Science Research Unit, University of Luxembourg, L-1511 Luxembourg

⁷*NEST, Scuola Normale Superiore and Istituto Nanoscienze-CNR, I-56126 Pisa, Italy*

Non-equilibrium states of quantum systems in contact with thermal baths help telling environments with different temperatures or different statistics apart. We extend these studies to a more generic problem that consists in discriminating between two baths with disparate constituents at unequal temperatures. Notably there exist temperature regimes in which the presence of coherence in the initial state preparation is beneficial for the discrimination capability. We also find that non-equilibrium states are not universally optimal, and detail the conditions in which it becomes convenient to wait for complete thermalisation of the probe. These concepts are illustrated in a linear-optical simulation.

I. INTRODUCTION

The reduced dynamics of a quantum system interacting with an external environment is typically insensitive to many characteristic features of the latter [1–3]. Yet some macroscopic properties of the bath (say its temperature) may have a non trivial influence on the resulting equations of motion, paving the way to the possibility of probing these quantities via measurements performed on the system alone [4–14].

Relying on these observations, in Ref. [15] a statistics tagging scheme has been presented, allowing to determine the fermionic or bosonic character of a thermal bath E by detecting the modifications induced on a quantum probing system A put in thermal contact with E for some proper interaction time t . The analysis was conducted assuming the temperature of the bath to be known and, most importantly, equal in the two alternative scenarios. Under this condition, waiting for the complete thermalization of A (i.e. setting $t \rightarrow \infty$) is clearly not a valuable option to get useful information on the nature of the bath: indeed as t diverges the probe will be driven toward the same final thermal equilibrium configuration irrespectively from the statistics of E , hence keeping no track of its fermionic or bosonic character. As a consequence the optimal discrimination performances in Ref. [15] were obtained at times t where the evolved state of A was explicitly in a non-equilibrium condition. Superiority of non-equilibrium conditions for measurement purposes are not unique to the statistics tagging procedure discussed in [15]: a similar behaviour can be observed in thermometric tasks, when we want to infer the temperature of a bosonic bath by the same interaction with a probe. Even if the thermalized states corresponding to different temperatures can be discriminated, there is an advantage when measuring the probe at earlier times [16–18]. Interestingly enough, the statistics tagging setting and the thermometric setting also

share another common feature: indeed in both schemes the input states of the probe which ensure optimal performances correspond to energy eigenstates of its local Hamiltonian, quantum coherence playing no fundamental role in the procedure (see however [8]). In an effort to check the generality of these observations (i.e. the optimality of using non-equilibrium observation times t and energy diagonal input states of the probe), here we cast the problem studied in Ref. [15] in a more complex framework by looking at the discrimination between two alternative thermal baths models which differ both in terms of their statistical properties *and* in terms of their associated temperatures. The analysis relies on information theoretical quantities which admit clear operational interpretations in quantum metrology [19–21]. In particular the minimization of the Helstrom probability of error [22] enables us to confirm that also for the generalized statistics tagging scenario we address here, optimal discrimination performances are obtained by monitoring the probe at times where it is in a non-equilibrium configuration. Yet in this case it turns out that such result strongly relies on the possibility of exploiting coherence in the input states of A : indeed when restricting the study to initial configurations of the probe with no coherence among the eigenstates of the system local Hamiltonian, we can exhibit explicit examples of the model parameters for which the best discrimination conditions are only met at equilibrium.

The paper is organized as follows: in Sec. II we introduce the model and present the figure of merit we are going to use in our analysis. Section III contains the main results of the paper discussing the role of coherent energy terms in the input state of the probe as well as the fact that non-equilibrium detection times are not always optimal if one restrict the analysis to initial configurations which are diagonal in the energy eigenbasis. In Sec. IV the previous concepts are illustrated in a linear optical simulator [23, 24]. The simulation allows to

mimic two different dissipative channels for a two level system [25]. In the typical tagging scenario, in which we have no a priori knowledge of which one of the channels is acting on the probe, we perform a set of measurements on the system and we reconstruct the original hypothesis via suitable statistical inference. In particular, we relied on a Bayesian technique [26] for constructing the error probabilities and providing a connection of this last with the theoretical figures mentioned above. Conclusions are presented in Sec. V while technical material is presented in the Appendix.

II. THE MODEL

The model we study can be schematized as follows. At time $t = 0$ a two-level (qubit) quantum probe A is prepared in some fiduciary initial density operator $\rho(0)$ and let interact for some time t with a partially unknown environment E that can be of two types: bosonic at temperature $1/\beta_b$, or fermionic at temperature $1/\beta_f$ (the values $1/\beta_b$ and $1/\beta_f$ being assigned a priori). As in Ref. [15] we shall attempt to discriminate among the two alternatives by only performing measurements on the reduced final state $\rho(t)$ of A , which hence encodes all the information about the nature of E one can access. This allows us to describe the whole scheme as a standard hypotheses testing problem [22] where one has to determine whether $\rho(t)$ corresponds to the density matrix $\rho_b(t)$ of A which one would have obtained by evolving $\rho(0)$ under the influence of the bosonic bath of temperature $1/\beta_b$, or to $\rho_f(t)$, which instead one would have obtained by evolving the same $\rho(0)$ under the influence of the fermionic bath of temperature $1/\beta_f$. To quantify our ability in discriminating between these scenarios we can then use the Helstrom error probability (HEP) functional

$$H(\rho_b(t), \rho_f(t)) := \frac{1}{2} - \frac{1}{4} \|\rho_b(t) - \rho_f(t)\|_1, \quad (1)$$

with $\|\cdots\|_1$ being the trace-norm symbol. This quantity, bounded between $[0, 1/2]$, provides the smallest probability of error one can get by optimizing over all possible measurements performed on a single copy of $\rho(t)$ [22]: accordingly, having $H(\rho_b(t), \rho_f(t)) = 0$ corresponds to perfect distinguishable configurations, while having $H(\rho_b(t), \rho_f(t)) = 1/2$ corresponds to absolutely indistinguishable configurations.

In order to get an analytical expression for (1) we assign $\rho_b(t)$ and $\rho_f(t)$ in terms two independent Gorini-Kossakowsky-Sudarshan-Lindblad master equations for A obtained under standard weak coupling system-bath assumptions [1, 2]. Moving into the interaction picture representation we write them as [15, 27, 28]

$$\dot{\rho}_q(t) = \gamma[1 + s_q \mathcal{N}_q(\beta_q)] \mathcal{D}_{\sigma_-}[\rho_q(t)] + \gamma \mathcal{N}_q(\beta_q) \mathcal{D}_{\sigma_+}[\rho_q(t)], \quad (2)$$

the index $q = f, b$ referring to the two hypothetical initial configurations of the bath. In the above expression $s_q = +(-)1$ for $q = b(f)$, γ is the inverse time constant associated to each elementary excitation/de-excitation process,

$$\mathcal{D}_{\sigma_{\pm}}[\cdots] := \sigma_{\pm}[\cdots] \sigma_{\pm}^{\dagger} - \frac{\sigma_{\pm}^{\dagger} \sigma_{\pm}[\cdots] + [\cdots] \sigma_{\pm}^{\dagger} \sigma_{\pm}}{2}, \quad (3)$$

represent the Lindblad dissipators associated respectively with the system ladder operators $\sigma_- = |0\rangle\langle 1|$ and $\sigma_+ = |1\rangle\langle 0|$ ($|0\rangle$ and $|1\rangle$ representing respectively the ground and excited state of A), while finally

$$\mathcal{N}_q(\beta_q) := \frac{1}{e^{\beta_q \omega} - s_q}, \quad (4)$$

is the Bose-Einstein (Fermi-Dirac) distribution for $q = b(f)$, with ω being an effective energy parameter [3, 28] that contains a contribution from the bare energy of A and from the chemical potential of the baths [29]. Introducing the Pauli vector operator $\vec{\sigma} := (\sigma_x, \sigma_y, \sigma_z)$, and writing the density matrix of the system in the Bloch vector formalism $\rho_q(t) = \frac{1 + \vec{\sigma} \cdot \vec{a}^{(q)}(t)}{2}$, Eq. (2) can then be conveniently casted in the form

$$\begin{aligned} \dot{a}_z^{(q)}(t) &= -\gamma_q a_z^{(q)}(t) - \xi_q, \\ \dot{a}_{x,y}^{(q)}(t) &= -\frac{\gamma_q}{2} a_{x,y}^{(q)}(t), \end{aligned} \quad (5)$$

where now

$$\begin{aligned} \gamma_b &:= \gamma \coth(\beta_b \omega / 2), & \gamma_f &:= \gamma, \\ \xi_b &:= \gamma, & \xi_f &:= \gamma \tanh(\beta_f \omega / 2), \end{aligned} \quad (6)$$

showing that in the case of equal temperatures, the evolution occurs at faster scales for the bosonic bath scenario. Explicit integration of (5) leads finally to the solution

$$\begin{aligned} a_z^{(q)}(t) &= e^{-\gamma_q t} (a_z(0) - a_z^{(q)}(\infty)) + a_z^{(q)}(\infty), \\ a_{x,y}^{(q)}(t) &= e^{-\gamma_q t/2} a_{x,y}(0), \end{aligned} \quad (7)$$

with $a_{x,y,z}(0)$ being the cartesian components of the Bloch vector associated with the input state $\rho(0)$ of A , while

$$a_z^{(q)}(\infty) = -\tanh(\beta_q \omega / 2), \quad (8)$$

defining the equilibrium (thermal) configuration of the system (of course $a_{x,y}^{(q)}(\infty) = 0$).

III. DISCRIMINATION PERFORMANCES

Using the fact that the trace-norm of the difference between $\rho_b(t)$ and $\rho_f(t)$ is just given by the Cartesian distance $|\vec{a}_b(t) - \vec{a}_f(t)|$ of the associated 3D Bloch vectors, from (7) it follows that Eq. (1) can be expressed as

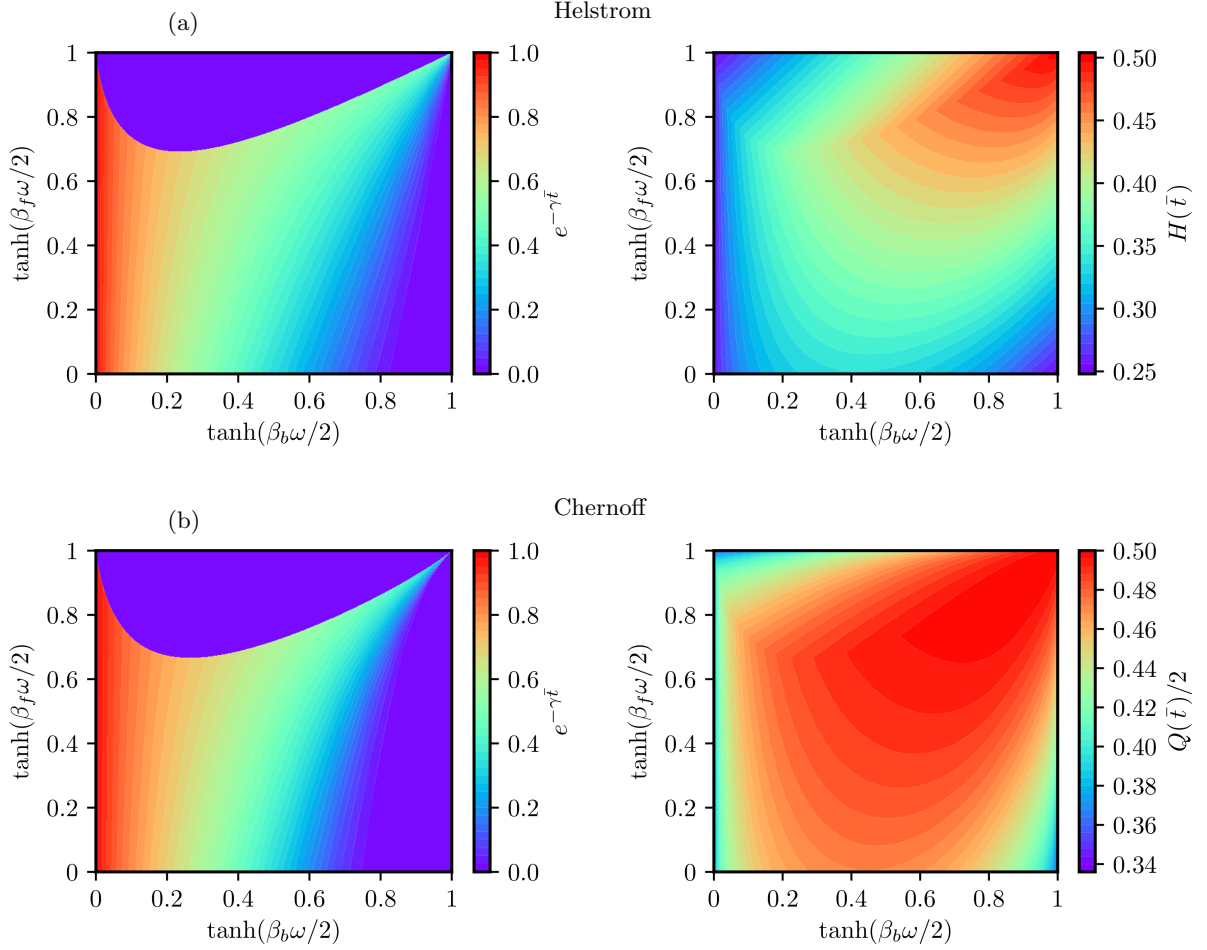


FIG. 1. Panel (a). Left: Study of the optimal measurement time \bar{t} minimizing the Helstrom error probability $H(t; 1)$ of Eq. (11) associated to the excited input state of the probe A (i.e. $a_z(0) = 1$), as a function of the bosonic and fermionic bath inverse temperatures β_b and β_f , using the convenient parametrizations indicated in the plot labels. The discontinuity in the contour plot is the boundary above which the discrimination is optimal only if performed on the steady state of the probe ($\bar{t} = \infty$, i.e. $e^{-\gamma\bar{t}} = 0$), the same holding for the pathological case $\beta_b = \infty$ ($\tanh(\beta_b\omega/2) = 1$). For all the other values of the parameters β_b and β_f the optimal time is finite ($\bar{t} < \infty$, i.e. $e^{-\gamma\bar{t}} > 0$). Right: Corresponding Helstrom probability of error $H(t; 1)$ evaluated at $t = \bar{t}$. Panel (b): same calculation as in (a) but using the Chernoff quantity (13) instead of the Helstrom error probability.

$$H(\rho_b(t), \rho_f(t)) = \frac{1}{2} - \frac{1}{4} \left\{ \left[(e^{-\gamma_f t} - e^{-\gamma_b t}) a_z(0) + a_z^{(f)}(\infty)(1 - e^{-\gamma_f t}) - a_z^{(b)}(\infty)(1 - e^{-\gamma_b t}) \right]^2 + (e^{-\gamma_f t/2} - e^{-\gamma_b t/2})^2 (|\vec{a}(0)|^2 - a_z^2(0)) \right\}^{1/2}. \quad (9)$$

A close inspection reveals that all pure input states $\rho(0)$ with the same initial value of $a_z(0)$ achieve the same performance (this simply follows from the symmetry of Eq. (5) around the z -axis). Furthermore for all assigned values of t and $a_z(0)$, one may notice that the associated HEP can be reduced by setting the length of $\vec{a}(0)$ at its maximum 1, i.e. imposing the initial state of the probe to be pure. This leads to

$$H(\rho_b(t), \rho_f(t)) \Big|_{\text{pure}} = H(t; a_z(0)) := \frac{1}{2} - \frac{1}{4} \left\{ \left[(e^{-\gamma_f t} - e^{-\gamma_b t}) a_z(0) + a_z^{(f)}(\infty)(1 - e^{-\gamma_f t}) - a_z^{(b)}(\infty)(1 - e^{-\gamma_b t}) \right]^2 + (e^{-\gamma_f t/2} - e^{-\gamma_b t/2})^2 (1 - a_z^2(0)) \right\}^{1/2}, \quad (10)$$

which only depends on the z -component $a_z(0) \in [-1, 1]$ of the unit vector $\vec{a}(0)$. It is worth recalling that fixing

$a_z(0) = 1$ ($a_z(0) = -1$) corresponds to initialize A into the excited state $|1\rangle$ (ground state $|0\rangle$) of its local Hamiltonian. On the contrary, in the pure case scenario we are facing in Eq. (10), the condition $|a_z(0)| < 1$ identifies input states of the probe which are proper superpositions of the energy eigenstates of the model. Our next goal is to minimize $H(t; a_z(0))$ with respect to all possible choices of $a_z(0)$ and of the evolution time t , for given values of the temperatures $1/\beta_f$ and $1/\beta_b$. Before doing so, however, we find useful to consider first what happens when

$a_z(0) = 1$, a choice that is known to provide the best discriminating strength for statistical tagging under equal bath temperature assumption (i.e. $\beta_f = \beta_b$) [15] and for thermometry [16].

A. Input excited state

Setting $a_z(0) = 1$, i.e. assuming A to be initialized in the excited state $|1\rangle$ of the model, Eq. (10) reduces to

$$H(t; 1) = \frac{1}{2} - \frac{1}{4} \left| e^{-\gamma_f t} - e^{-\gamma_b t} + a_z^{(f)}(\infty)(1 - e^{-\gamma_f t}) - a_z^{(b)}(\infty)(1 - e^{-\gamma_b t}) \right|, \quad (11)$$

which we minimize numerically with respect to t as a function of β_f and β_b . The optimal times \bar{t} we obtain and the corresponding values of $H(\bar{t}; 1)$ are reported in Fig. 1(a) (left and right plots, respectively). The plot reveals an asymmetry: for $\beta_b \geq \beta_f$ (fermion bath hotter than bosonic bath) the best discrimination is still attained at finite time ($\bar{t} < \infty$) where A has not achieved full thermalization and is hence in a non-equilibrium configuration in line with the findings of Ref. [15]; on the contrary for $\beta_b < \beta_f$ (fermion bath cooler than bosonic bath) it can be more convenient to discriminate the two channels by exploiting the steady state properties ($\bar{t} = \infty$). This happens above the critical curve that defines the discontinuity in the left contour plot of Fig. 1(a). An analytical treatment of this transition is given in Appendix A, from which it results that expressed in the $x = \tanh(\beta_f \omega/2)$, $y = \tanh(\beta_b \omega/2)$ coordinates of Fig. 1, such critical curve is identified by solving the following set of transcendental equations

$$\begin{cases} (2 - e^{-\tau})(1 + x) - (2 - e^{-\frac{\tau}{y}})(1 + y) = 0, \\ e^{-\tau}(1 + x) - e^{-\frac{\tau}{y}}y^{-1}(1 + y) = 0, \end{cases} \quad (12)$$

with $\tau \geq 0$. We remark that the core of the above observation remains unchanged when we evaluate the discrimination efficiency of the process adopting different figures of merit. For instance in Fig 1(b) we focus on the Chernoff quantity [30, 31]

$$Q(\rho_b(t), \rho_f(t)) := \min_{r \in [0, 1]} \text{Tr}[\rho_b^r(t) \rho_f^{1-r}(t)], \quad (13)$$

which via the inequality

$$H(\rho_b^{\otimes N}(t), \rho_f^{\otimes N}(t)) \leq \frac{Q(\rho_b(t), \rho_f(t))^N}{2}, \quad (14)$$

gives a bound to the asymptotic rate of HEP computed in the case when one has the possibility of extracting information from N identical copies of the final state of A . The optimal values of \bar{t} obtained by numerically minimizing (13) when initializing A in the excited state $|1\rangle$, are presented in Fig 1(b) exhibiting a critical trade-off

analogous to the one observed in Fig 1(a): if we restrict the analysis to the case where A is set into the excited state there are configurations of the model where the optimal discrimination efficiency is attained only letting the system to reach its equilibrium configuration.

B. Optimal input states of the probe

In this section we now exploit the full domain of possibilities offered by the model, minimizing the HEP value (10) not just with respect to t , but also with respect to the full domain of $a_z(0)$, hence including the possibility of using input states of A which explicitly exhibit coherence superpositions among the excited and ground state of the model. An indication that such special states could be of some help in improving the performance of the scheme follows by observing that for $|a_z(0)| < 1$ it is not possible to find times $t > 0$ such that $H(t; a_z(0))$ reaches the worst case value of $1/2$ corresponding to an absolute impossibility of distinguishing among the two bath scenarios. This implies that coherent energy input states ensure a non-trivial susceptibility of the probe for all choices of t , something that, on the contrary, is not generally granted by setting $a_z(0) = \pm 1$ which, as discussed in Appendix B 1, allows for crossing points between the trajectories $\rho_b(t)$ and $\rho_f(t)$. Values of $|a_z(0)| < 1$ can however do much more than this and in some regimes, they also give the absolute best performance we can aim to: the details of the analysis are provided in Appendix B 2 while in Fig. 2 we illustrate the optimization of the HEP $H(t; a_z(0))$ over time and input state of the probe, as a function of the bath inverse temperatures β_f and β_b .

The first thing to be noticed is that now, at variance with the input excited state case discussed in Sec. III A, the optimal times \bar{t} are always finite apart from the asymptotic regimes where the bosonic temperature converges to zero (i.e. $\beta_b \rightarrow \infty$) – compare Fig. 2 (a) with the left plot of Fig. 1 (a). This shows that optimality of non-equilibrium probing times is fully restored once we do not restrict the probe input state to specific condi-

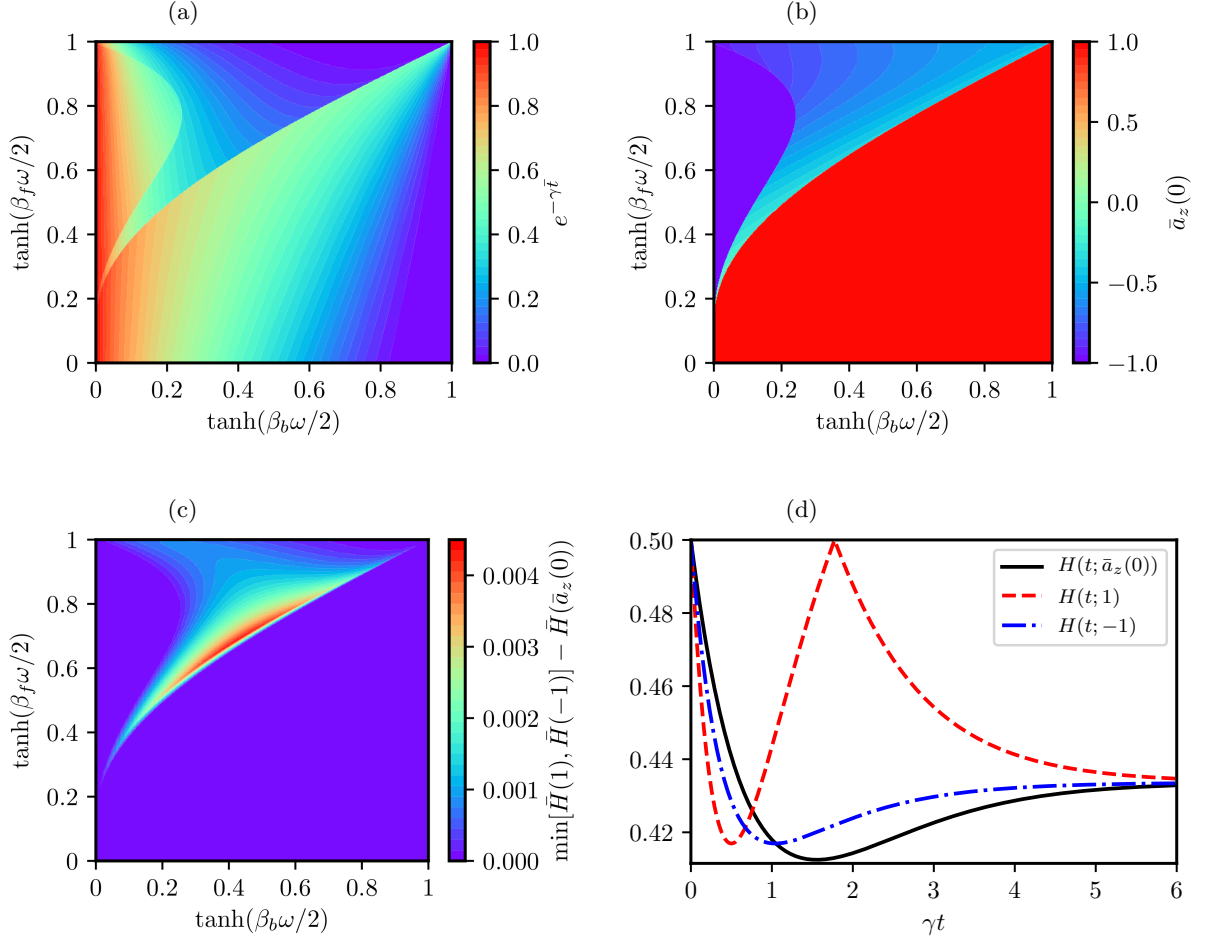


FIG. 2. Panels (a)-(c): Optimization of the HEP $H(t; a_z(0))$ of Eq. (10) both over time and over the input state of the probe, the last being a generic pure state with a certain value $a_z(0)$ of the z-component of the Bloch vector. We report the following contour plots with respect to the bath inverse temperatures β_f and β_b . The minimum $\bar{H}(\bar{a}_z(0))$ of the HEP is achieved at a certain time \bar{t} (a) and for an optimal value $\bar{a}_z(0)$ of $a_z(0)$ (b). The advantage coming from allowing coherent superpositions is presented in (c), where we show the gap between the (generally overestimated) quantity obtained by restricting the analysis only to $a_z(0) \in \{1, -1\}$ and the optimal value $\bar{H}(\bar{a}_z(0))$. Notice that for β_f , β_b and \bar{t} we used the convenient parametrizations indicated in the plot labels. Panel (d): dynamical evolution of $H(t; a_z(0))$ for a case ($\tanh(\beta_f \omega/2) \approx 0.68$, $\tanh(\beta_b \omega/2) \approx 0.41$) in which coherent superpositions ($\bar{a}_z(0) \approx -0.42$) give better performances than the energy eigenstates ($a_z(0) \in \{1, -1\}$) as input of the probe. Notice that at $t \approx 1.8\gamma^{-1}$ the HEP associated with excited state reaches the worst case value $1/2$ indicating zero susceptibility of the probe.

tions. There, we can expect that coherence properties of the probe become even more relevant, thus richness and complexity to the observable phenomenology. (citiamo engine squeezed)

energy eigenstates (either excited or ground states) of the probe as input is optimal for most of the choices of the system parameter setting, there is a non trivial temperatures regime in which a coherent ($|a_z(0)| < 1$) initial preparation is fundamental to reach the best performance. More specifically, there is numerical evidence that whenever the fermionic bath is hotter than the bosonic one ($\beta_b \geq \beta_f$), choosing the excited state of A as input is still the right choice to provide optimal discrimination performances. The situation changes how-

ever if the fermionic bath is cooler than the bosonic one ($\beta_b < \beta_f$): here the optimal input choice depends on the specific values of the temperature and in particular for sufficiently large β_f coherent energy states dominate (notice also that for β_f small the optimal input is the ground state of A). These facts are also enlightened in Fig. 2 (c) in which we show the gap between the minimum of $H(t; a_z(0))$ obtained by restricting the optimization only to $a_z(0) = 1$ and $a_z(0) = -1$ and the optimal value $\bar{H}(\bar{a}_z(0))$ obtained by allowing also energy coherent preparations.

In panel (d) of Fig. 2 we finally present as an example the temporal evolution of the HEP for a specific choice of the temperatures that admits as optimal the value

$\bar{a}_z(0) \approx -0.42$ that identifies a coherent superposition of energy eigenstates. In such a plot we show $H(t; \bar{a}_z(0))$ aside with the HEP values $H(t; -1)$ and $H(t; 1)$ associated with the ground and excited input state of A . Notice that while for small t , $H(t; -1)$ and $H(t; 1)$ perform better than $H(t; \bar{a}_z(0))$, in the long run the latter gives the lowest HEP values and leads to the identification of the optimal time as $\bar{t} \approx 1.6\gamma^{-1}$ – see Appendix for more on this. Notice also that at $t \approx 1.8\gamma^{-1}$, we have $H(t; 1) = 1/2$ indicating that at this special time the probe initialized into the excited state loses all its ability in discriminating between the two alternative hypothesis: on the contrary, as anticipated in the introductory paragraphs of the section, $H(t; \bar{a}_z(0))$ remains strictly below the $1/2$ value for all positive t .

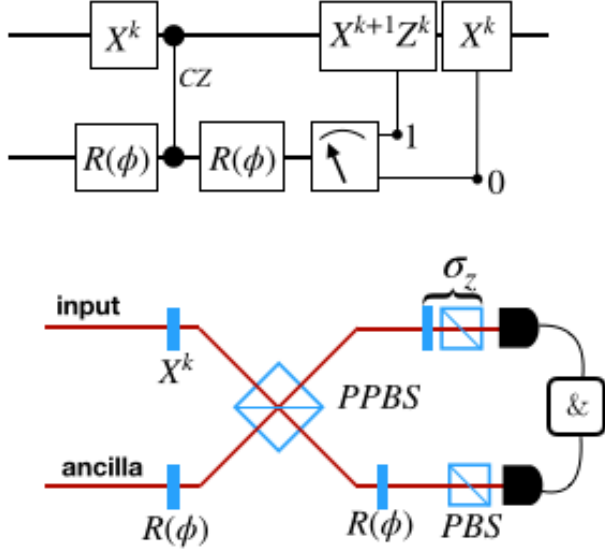


FIG. 3. Linear optical simulator. The state at time τ can be simulated by mixing with weights w_k the actions of two channels ($k = 0$ and $k = 1$), associated to excitation and de-excitation processes, for a given rotation $R(\phi)$ (upper panel). By tuning w_k and ϕ evolutions at different temperatures and at variable times are simulated [23, 24]. This is implemented in a linear-optical setup, based on polarisation coding on two photons from a down-conversion source (lower panel). Single-qubit operations are either implemented by half-wave plates, or in post-processing of the data. The input state is fixed in the horizontal polarisation. Due to the use of a single partially polarising beam splitter (PPBS), there is a different transmission probability for the horizontal and vertical components, which is compensated by biasing the second $R(\phi)$ rotation [32]. Further, the weights w_k have to be modified accordingly.

IV. DISCRIMINATION EXPERIMENT IN AN OPTICAL SIMULATOR

We can illustrate these concepts in a simulated thermalisation, carried out with a pair of qubits; the necessary gate is implemented by means of optical elements and coincidences counts. The setup, illustrated in Fig. 3, follows closely our previous work in Ref. [23]. We stress that our simulator cannot replicate directly the bosonic/fermionic nature of the bath; the control parameters are exclusively the decay rates γ_f or γ_b in Eq. (5), and the population of the final thermal state. In this respect, our implementation is a synthesis of the output state. Therefore, we focus on the information content of the probe, rather than the interaction process.

We consider a two level system initialized in the excited state as the input probe. The expectation values of σ_z measured as a function of the normalized time $\tau = \gamma t$ are shown in Fig. 4 for different inverse temperatures $\beta\omega = 0.5, 1, 2$, taken equal for fermionic and bosonic baths. The two different curves in each panel illustrate how the decay rate of the probe state gets modified by the two different statistics.

In a discrimination experiment, the sought outcome is a binary decision on which one of the two hypotheses gives a closer description of the data [33–38]. These will be obtained as outcomes of a suitable observable, selected according to the initial state and the measurement time. For our choice of initial state, this observable always coincides with σ_z . In many different (and independent) runs of the experiment, one collects N_0 events for the eigenvalue -1 and N_1 events for the eigenvalue $+1$ of σ_z . Since the probabilities of obtaining either result on a single copy are $P_i = (1 + (-1)^{i+1}\langle\sigma_z\rangle^{(q)}(t))/2$, where the value of $\langle\sigma_z\rangle^{(q)}$ is the expectation value predicted by the experiment, the composite probability is $\mathbf{P} = P_0^{N_0} P_1^{N_1}$.

Clearly, the probability \mathbf{P} depends on the bath statistics and temperature through the expectation value $\langle\sigma_z\rangle$. We can thus interpret \mathbf{P} as a conditioned probability $\mathbf{P}(N_0, N_1|X)$ of the whole experimental run, given the condition X of the bath. Invoking Bayes theorem this writes:

$$\mathbf{P}(X|N_0, N_1) = \frac{1}{\mathcal{N}} \mathbf{P}(N_0, N_1|X) P(X), \quad (15)$$

where \mathcal{N} is a normalization constant and $P(X)$ is the *a priori* probability which we take to be flat $P(b) = P(f) = 1/2$. The decision criterion is that when $P(b|N_0, N_1) > P(f|N_0, N_1)$, the bath is identified as bosonic with inverse temperature β_b , otherwise as fermionic with inverse temperature β_f .

In accordance with the literature [22, 39], we quantify the expected discrimination error as:

$$\delta = \frac{1}{2} \left(P(b, \beta_b|N_0^{f, \beta_f}, N_1^{f, \beta_f}) + P(f, \beta_f|N_0^{b, \beta_b}, N_1^{b, \beta_b}) \right), \quad (16)$$

where we have fixed $N_i^{q, \beta_q} = P_i \cdot N$, ($N=10, 100$) as the ideal limit. The first case we analyse is that of statis-

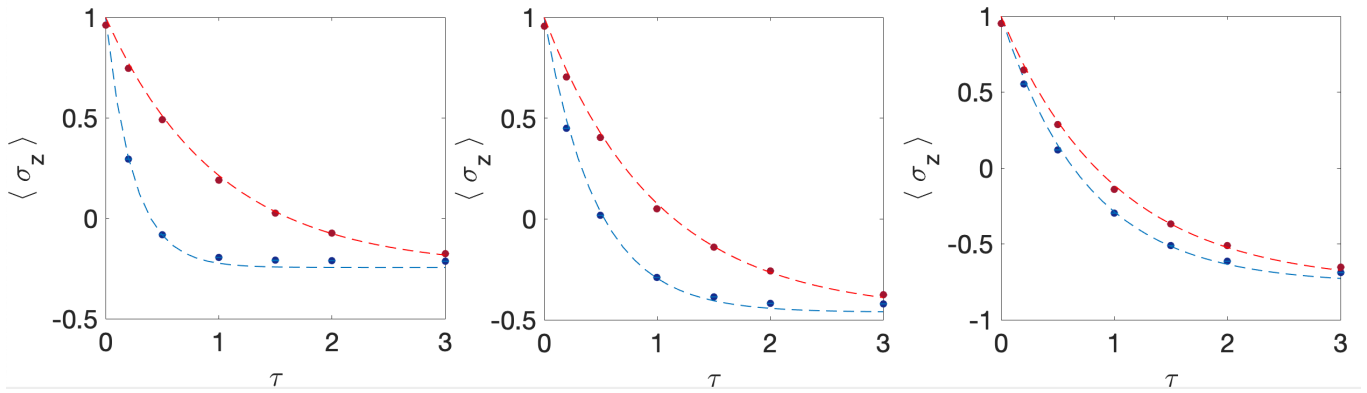


FIG. 4. Simulated thermalization dynamics of the probe initialized in the excited state. The behaviour of the expectation value $\langle \sigma_z \rangle$ as a function of the time $\tau = \gamma t$ is reported for $(\omega \equiv 1)$ $\beta_b = \beta_f = 0.5, 1, 2$ (left, middle, and right panel, respectively). Blue (red) experimental points refer to the bosonic (fermionic) statistics of the bath. Error bars are smaller than the size of the points.

tical tagging $\beta_b = \beta_f$, for which optimal discrimination necessarily occurs at finite times. In Fig. 5 we show the behaviour of δ for $\beta_b = \beta_f$. We notice that the small discrepancies observed with respect to the theory do not affect the estimation significantly. It appears evident how, for high temperatures, the choice of a preferable discrimination time becomes less strict with increasing copies N . On the other hand, the proximity of the two curves in Fig. 4(c) is reflected in the fact that at low temperatures more copies are needed for a fully reliable discrimination.

Concerning the more general scenario of different temperatures and statistics, we have evaluated δ for all permutations of $\beta\omega = 0.5, 1, 2$ and for $N = 10, 100$ in the same ideal limit as above. The results are shown in Fig. 6. Notably, for $\beta_b < \beta_f$ there is a special time instant where the discrimination is impossible, in analogy to what we obtained for the HEP - see Panel (d) of Fig. 2. This can be observed in Panels (a), (b) and (d) of Fig. 6 where, contrarily to the other Panels, δ takes the value $1/2$ at an intermediate time. We report in Fig. 7 contour plots showing the calculation of the optimal measurement time and of the corresponding minimized error probability when using the Bayesian method in the ideal situation. Consistently, the results mimic the ones obtained via Helstrom and Chernoff approaches - see Fig. 1.

We then carry out the actual discrimination protocol as follows. We generate, based on the experimental values of P_0 and P_1 a vector of $N = 100$ outcomes $0, 1$ [40]. This is a reliable evaluation of our experimental conditions, as the data are marginally affected by systematic errors such as dark counts, and we are considering samples much smaller than those collected to estimate P_0 and P_1 in the calibration step. The results are reported, for a vector of $N = 100$ generated outcomes, in the histograms of Fig. 8 for different choices of scenarios, considering both instances in which the probe is associated to a bosonic or a fermionic bath, in accordance to the fact that the error δ is symmetrised.

For each simulated time τ we indicate with different

colours the fraction of events in which the bath has been correctly identified (blue) or mistaken (red) by following the Bayesian decision rule explained above - now with the actual values of N_0 and N_1 , rather than their expected ones. The observed behaviours qualitatively mirror the errors in Figs. 5 and 6. Since N_0 and N_1 are now random variables, the discrimination capability exhibits deviations from the expected case.

V. CONCLUSIONS

Statistical tagging [15] and, more generally, bath discrimination, is a simple yet insightful instance of the possibility of indirectly probing an environment [4–14, 41]. In this setting, information about the bath structure are retrieved via measurements on a quantum probe which has interacted with the bath up to a selected measurement time \bar{t} . This approach reveals how different properties of the bath affect the nature of the optimal discrimination procedures. This is clear in the tagging context presented here: a thermal bath has an unknown statistics - fermionic or bosonic - that we want to guess, with the additional information of knowing the respective temperatures - $1/\beta_f$ and $1/\beta_b$ - associated to the two bath instances. Here the quantum nature of the problem is manifested both in the statistical properties of the bath and in the coherence of the single-qubit probe. For input energy eigenstates, our inspection has revealed a transition between temperature regimes in which either equilibrium - $\bar{t} \rightarrow \infty$ - or non-equilibrium states - $\bar{t} < \infty$ - are optimal. Such behavior has been illustrated both theoretically and in a linear-optical simulation. States with quantum coherence, instead, do not display such transition - i.e. non-equilibrium conditions are generally optimal - and their inclusion allows to reach the best discrimination capability. Extensions of this work may concern baths with richer features, such as very large baths presenting squeezing

or, to the other extreme, small environments, entailing more involved treatments. There, we can expect coherence properties of the probe to become even more relevant, thus adding richness and complexity to the observable phenomenology.

D.F. and V.G. acknowledge support from PRIN 2017

“Taming complexity with quantum strategies”. During the completion of this manuscript, the authors became aware of a related work in preparation by L. Mancino et al. “Non-equilibrium readiness and accuracy of Gaussian Quantum Thermometers” also dealing with metrological tasks by means of indirectly measuring environments via quantum probes.

-
- [1] G. Lindblad, On the generators of quantum dynamical semigroups, *Communications in Mathematical Physics* **48**, 119 (1976).
 - [2] V. Gorini, A. Kossakowski, and E. C. G. Sudarshan, Completely positive dynamical semigroups of N-level systems, *Journal of Mathematical Physics* **17**, 821 (1976).
 - [3] H.-P. Breuer and F. Petruccione, *The Theory of Open Quantum Systems* (Oxford University Press, 2002).
 - [4] M. Brunelli, S. Olivares, and M. G. A. Paris, Qubit thermometry for micromechanical resonators, *Phys. Rev. A* **84**, 032105 (2011).
 - [5] L. A. Correa, M. Mehboudi, G. Adesso, and A. Sanpera, Individual quantum probes for optimal thermometry, *Phys. Rev. Lett.* **114**, 220405 (2015).
 - [6] A. De Pasquale, K. Yuasa, and V. Giovannetti, Estimating temperature via sequential measurements, *Phys. Rev. A* **96**, 012316 (2017).
 - [7] S. Campbell, M. G. Genoni, and S. Deffner, Precision thermometry and the quantum speed limit, *Quantum Science and Technology* **3**, 025002 (2018).
 - [8] A. H. Kiilerich, A. De Pasquale, and V. Giovannetti, Dynamical approach to ancilla-assisted quantum thermometry, *Phys. Rev. A* **98**, 042124 (2018).
 - [9] M. Schlosshauer, A. P. Hines, and G. J. Milburn, Decoherence and dissipation of a quantum harmonic oscillator coupled to two-level systems, *Phys. Rev. A* **77**, 022111 (2008).
 - [10] J. P. Pekola, S. Suomela, and Y. M. Galperin, Finite-size bath in qubit thermodynamics, *Journal of Low Temperature Physics* **184**, 1015 (2016).
 - [11] S. Gröblacher, A. Trubarov, N. Prigge, G. D. Cole, M. Aspelmeyer, and J. Eisert, Observation of non-markovian micromechanical brownian motion, *Nature Communications* **6**, 7606 (2015).
 - [12] N. V. Prokof'ev and P. C. E. Stamp, Theory of the spin bath, *Reports on Progress in Physics* **63**, 669 (2000).
 - [13] A. De Pasquale, D. Rossini, R. Fazio, and V. Giovannetti, Local quantum thermal susceptibility, *Nature Communications* **7**, 12782 (2016).
 - [14] C. Benedetti, F. Salari Sehdaran, M. H. Zandi, and M. G. A. Paris, Quantum probes for the cutoff frequency of Ohmic environments, *Phys. Rev. A* **97**, 012126 (2018).
 - [15] D. Farina, V. Cavina, and V. Giovannetti, Quantum bath statistics tagging, *Phys. Rev. A* **100**, 042327 (2019).
 - [16] S. Jevtic, D. Newman, T. Rudolph, and T. M. Stace, Single-qubit thermometry, *Phys. Rev. A* **91**, 012331 (2015).
 - [17] W. K. Tham, H. Ferretti, A. V. Sadashivan, and A. M. Steinberg, Simulating and optimising quantum thermometry using single photons, *Scientific Reports* **6**, 38822 (2016).
 - [18] L. Mancino, M. Sbroscia, I. Gianani, E. Roccia, and M. Barbieri, Quantum simulation of single-qubit thermometry using linear optics, *Phys. Rev. Lett.* **118**, 130502 (2017).
 - [19] V. Giovannetti, S. Lloyd, and L. Maccone, Quantum metrology, *Phys. Rev. Lett.* **96**, 010401 (2006).
 - [20] M. G. Paris, Quantum estimation for quantum technology, *Int. J. Quantum Inform.* **7**, 125 (2009).
 - [21] V. Giovannetti, S. Lloyd, and L. Maccone, Advances in quantum metrology, *Nature photonics* **5**, 222 (2011).
 - [22] C. W. Helstrom, *Quantum detection and estimation theory*, (Academic Press, New York, 1976).
 - [23] L. Mancino, V. Cavina, A. De Pasquale, M. Sbroscia, R. I. Booth, E. Roccia, I. Gianani, V. Giovannetti, and M. Barbieri, Geometrical bounds on irreversibility in open quantum systems, *Phys. Rev. Lett.* **121**, 160602 (2018).
 - [24] V. Cavina, L. Mancino, A. De Pasquale, I. Gianani, M. Sbroscia, R. I. Booth, E. Roccia, R. Raimondi, V. Giovannetti, and M. Barbieri, Bridging thermodynamics and metrology in nonequilibrium quantum thermometry, *Phys. Rev. A* **98**, 050101 (2018).
 - [25] H. Lu, C. Liu, D.-S. Wang, L.-K. Chen, Z.-D. Li, X.-C. Yao, L. Li, N.-L. Liu, C.-Z. Peng, B. C. Sanders, Y.-A. Chen, and J.-W. Pan, Experimental quantum channel simulation, *Phys. Rev. A* **95**, 042310 (2017).
 - [26] M. G. Genoni, S. Olivares, D. Brivio, S. Cialdi, D. Cipriani, A. Santamato, S. Vezzoli, and M. G. A. Paris, Optical interferometry in the presence of large phase diffusion, *Phys. Rev. A* **85**, 043817 (2012).
 - [27] D. Farina and V. Giovannetti, Open-quantum-system dynamics: Recovering positivity of the redfield equation via the partial secular approximation, *Phys. Rev. A* **100**, 012107 (2019).
 - [28] K. L. Massimiliano Esposito, Ryoichi Kawai and C. V. den Broeck, Quantum-dot carnot engine at maximum power, *Phys. Rev. E* **81**, 041106 (2010).
 - [29] We suppose ω to be the same for b and f . When the chemical potential is different between the fermionic and bosonic cases we can opportunely redefine β_f and β_b to preserve the Eq. (4).
 - [30] K. M. R. Audenaert, J. Calsamiglia, R. Muñoz Tapia, E. Bagan, L. Masanes, A. Acín, and F. Verstraete, Discriminating states: The Quantum Chernoff Bound, *Phys. Rev. Lett.* **98**, 160501 (2007).
 - [31] J. Calsamiglia, R. Muñoz Tapia, L. Masanes, A. Acín, and E. Bagan, Quantum Chernoff bound as a measure of distinguishability between density matrices: Application to qubit and Gaussian states, *Phys. Rev. A* **77**, 032311 (2008).
 - [32] B. P. Lanyon, T. J. Weinhold, N. K. Langford, M. Barbieri, D. F. V. James, A. Gilchrist, and A. G. White, Experimental demonstration of a compiled version of shor's

- algorithm with quantum entanglement, Phys. Rev. Lett. **99**, 250505 (2007).
- [33] P. J. Mosley, S. Croke, I. A. Walmsley, and S. M. Barnett, Experimental realization of maximum confidence quantum state discrimination for the extraction of quantum information, Phys. Rev. Lett. **97**, 193601 (2006).
- [34] G. J. Pryde, J. L. O'Brien, A. G. White, and S. D. Bartlett, Demonstrating superior discrimination of locally prepared states using nonlocal measurements, Phys. Rev. Lett. **94**, 220406 (2005).
- [35] S. Slussarenko, M. M. Weston, J.-G. Li, N. Campbell, H. M. Wiseman, and G. J. Pryde, Quantum state discrimination using the minimum average number of copies, Phys. Rev. Lett. **118**, 030502 (2017).
- [36] M. Bina, A. Allevi, M. Bondani, and S. Olivares, Homodyne-like detection for coherent state-discrimination in the presence of phase noise, Opt. Express **25**, 10685 (2017).
- [37] M. T. DiMario, E. Carrasco, R. A. Jackson, and F. E. Becerra, Implementation of a single-shot receiver for quaternary phase-shift keyed coherent states, J. Opt. Soc. Am. B **35**, 568 (2018).
- [38] F. E. Becerra, J. Fan, and A. Migdall, Implementation of generalized quantum measurements for unambiguous discrimination of multiple non-orthogonal coherent states, Nature Communications **4**, 2028 (2013).
- [39] M. A. Nielsen and I. Chuang, Quantum computation and quantum information (2002).
- [40] This is achieved by generating a random number r uniformly between 0 and 1; if $r < P_0$, then N_0 is incremented by one unit (starting from $N_0 = N_1 = 0$), otherwise N_1 is incremented.
- [41] M. Mehboudi, A. Lampo, C. Charalambous, L. A. Correa, M. A. García-March, and M. Lewenstein, Using polarons for sub-nk quantum nondemolition thermometry in a Bose-Einstein condensate, Phys. Rev. Lett. **122**, 030403 (2019).

A. Excited input state

Equation (1) clearly shows that the minimal values of HEP are achieved when $\|\rho_b(t) - \rho_f(t)\|_1$ gets maximum. From Eq. (11) it follows that for the case of excited input state, i.e. for $a_z(0) = 1$, this quantity can be expressed as

$$\|\rho_b(t) - \rho_f(t)\|_1 = D(t, x, y) := |(1 - e^{-\gamma t})(1 + x) - (1 - e^{-\frac{\gamma t}{y}})(1 + y)|, \quad (17)$$

where, for ease of notation, we introduced

$$x := -a_z^{(f)}(\infty) = \tanh(\beta_f \omega / 2), \quad y := -a_z^{(b)}(\infty) = \tanh(\beta_b \omega / 2), \quad (18)$$

and explicited $\gamma_f = \gamma$, $\gamma_b = \gamma/y$. Studying the Eq. (17) as a function of t we can infer which instant is optimal to perform a single measurement for discriminating between the two hypotheses.

As first, we notice that $D(t, x, y)$ nullifies at $t = 0$ (obviously) and at most in another point, since by solving $D(t, x, y) = 0$ we have

$$\frac{1+x}{1+y} = \frac{1 - e^{-\frac{\gamma t}{y}}}{1 - e^{-\gamma t}}. \quad (19)$$

The unicity of the solution can be argued using the monotonicity of the *r.h.s.* of Eq. (19). Notice that the other solution (at $t = 0$) cannot be obtained from Eq. (19) since we divided by $(1 - e^{-\gamma t})$ that nullifies in that case. The first derivative of $D(t, x, y)$ with respect to time reads

$$D'(t) = \gamma \text{sign}[(1 - e^{-\gamma t})(1 + x) - (1 - e^{-\frac{\gamma t}{y}})(1 + y)]((1 + x)e^{-\gamma t} - (1 + y)y^{-1}e^{-\frac{\gamma t}{y}}), \quad (20)$$

that clearly nullifies in the long time limit $\gamma t \rightarrow \infty$. To find other zeroes of D' we have to solve the following equation

$$\frac{1+x}{1+y^{-1}} = e^{-\gamma t(y^{-1}-1)}, \quad (21)$$

that can have at most one solution since the *r.h.s.* is a strictly decreasing function. In addition, it is possible to prove that, calling t_1 and t_2 the zeroes at finite time respectively of $D(t, x, y)$ and of its first derivative, we have $t_1 \geq t_2$. Indeed they satisfy the two equations (19) and (21) from which we derive

$$\frac{e^{-\gamma t_2(y^{-1}-1)}}{y} = \frac{1 - e^{-\frac{\gamma t_1}{y}}}{1 - e^{-\gamma t_1}}. \quad (22)$$

Now we can use the following inequality: $\frac{e^{-\gamma t_2(y^{-1}-1)}}{y} \leq \frac{1 - e^{-\frac{\gamma t_2}{y}}}{1 - e^{-\gamma t_2}}$, from which $t_1 \geq t_2$ can be argued using the decreasing properties of both sides of Eq. (22).

As a last step we want to study the behaviour of the zeroes in the parameters x, y . It is straightforward to verify that Eq. (17) has no solutions if $x < y$, since there is no crossing between the bosonic and fermionic evolutions in this case. Notice that, following the definition of x and y , this last condition is equivalent to require the inverse temperature β_f in the fermionic case to be lower than the one in the bosonic case β_b . Notice instead that the Eq. (21) always nullifies once, independently from the value of x, y . In conclusion, we have two possible qualitative trends for the trace norms (17):

1. If $\beta_f < \beta_b$, $D(t)$ starts from 0 and never nullifies again. The derivative of D is zero once, in such a way that there is one single maximum. This case includes the analysis done in [15] in which $\beta_f = \beta_b$ was considered.
2. If $\beta_f > \beta_b$, $D(t)$ reaches a maximum in t_2 , then decreases to a point t_1 in which attains the value 0. After t_1 $D(t)$ starts increasing again and remain monotonous when going to infinity.

1. Analysis of the critical point

For the sake of characterizing the optimal measurements, we should find the maxima of the trace norm studied in the previous section. In the case $\beta_f < \beta_b$ there is only one maximum, and the measurement should be clearly done in the instant of time associated to that maximum. In the case $\beta_f > \beta_b$ the intermediate maximum could be both greater or lesser than the value attained by $D(t)$ at infinitely long times. In the following we will show that, again in dependence on the values assumed by the inverse temperatures β_f and β_b , either one or the other strategy can be the best one.

To give a clear formulation to this question from a formal point of view, let us define the following function

$$g(t, x, y) = D(t) - \lim_{t \rightarrow \infty} D(t). \quad (23)$$

The zeroes of the function defined above correspond to the points in which $D(t)$ attains the same value as it does at $t = \infty$. Thus, if the equation $g(t, x, y) = 0$ has no solutions, the absolute maximum is clearly located at $t \rightarrow \infty$. Otherwise, given the properties of $D(t)$ enumerated in the previous section, the function $g(t, x, y)$ can have at most two zeroes, depending on the values of x and y . In this last case, the maximum is not located at $t = \infty$, since this last point is equal to at most two other values that the function $D(t)$ attains at finite time. It is also understood that the points in which $g(t, x, y)$ has a unique zero (that will be referred from now as *critical*) are the ones in which $D(t)$ has two absolute maxima (identical in value). If we fix the value of y to some value \bar{y} , we have that in a critical point the solution $x_c(t, \bar{y})$ of $g(t, x, \bar{y}) = 0$ must be such that $\frac{\partial}{\partial t} x(t, \bar{y}) = 0$ evaluated in the critical point (this last property is derived from the regularity of g and the definition of critical point, in which the Eq. $g(t, x, y) = 0$ passes from having zero to two solutions). We can then derive, using the definition of g , the following set of equations for the critical point

$$\begin{aligned} (2 - e^{-\gamma t})(1 + x) - (2 - e^{-\frac{\gamma t}{\bar{y}}})(1 + \bar{y}) &= 0, \\ e^{-\gamma t}(1 + x) - e^{-\frac{\gamma t}{\bar{y}}}\bar{y}^{-1}(1 + \bar{y}) &= 0, \end{aligned} \quad (24)$$

that replacing γt with τ gives the Eq. (12) of the main text. For instance, choosing $\bar{y} = 1/2$ we have $x_c = \frac{2\sqrt{2}-1}{\sqrt{2}+1}$ and $t_c = \log(\frac{\sqrt{2}+1}{\sqrt{2}})$. Then, if we choose $x < x_c$ the better strategy is to measure at finite time, while if $x > x_c$ the measurement at the steady state is the optimal one.

B. Discrimination with generic pure input states

Here we proceed with an analytical analysis of the HEP functional $H(t; a_z(0))$ defined in Eq. (10).

1. Loss of susceptibility under non-coherent inputs

The worst discrimination scenario is attained when HEP reaches its maximum value 1/2: when this happens the probability of error is maxima and we cannot recover information on the nature of the bath from the state of A . From

Eq. (1) this happens when $\|\rho_b(t) - \rho_f(t)\|_1 = 0$, i.e. when the two trajectories intercept. From Eq. (10) we observe that this can only occur when

$$\begin{cases} (e^{-\gamma_f t/2} - e^{-\gamma_b t/2})^2 (1 - a_z^2(0)) = 0, \\ (e^{-\gamma_f t} - e^{-\gamma_b t})a_z(0) + a_z^{(f)}(\infty)(1 - e^{-\gamma_f t}) - a_z^{(b)}(\infty)(1 - e^{-\gamma_b t}) = 0. \end{cases} \quad (25)$$

However setting $|a_z(0)| < 1$, i.e. allowing the input state of A to be a non trivial superposition of the energy eigenstates, this corresponds to

$$\begin{cases} e^{-\gamma_f t/2} = e^{-\gamma_b t/2}, \\ (a_z^{(f)}(\infty) - a_z^{(b)}(\infty))(1 - e^{-\gamma_b t}) = 0, \end{cases} \quad (26)$$

which can only be fulfilled for $t = \infty$ and $\beta_f = \beta_b$. On the contrary setting $a_z(0) = \pm 1$ (i.e forcing the probe to be in one of the two eigenstates of the system), the system (25) reduces to a single equation

$$\pm(e^{-\gamma_f t} - e^{-\gamma_b t}) + a_z^{(f)}(\infty)(1 - e^{-\gamma_f t}) - a_z^{(b)}(\infty)(1 - e^{-\gamma_b t}) = 0, \quad (27)$$

which, depending on the specific values of β_b and β_f may allow for non trivial $t > 0$ solutions, i.e. indicating a loss of susceptibility of the probe.

2. Full optimization

We are interested in determining the minimum value of Eq. (10) with respect to all possible inputs (i.e. all possible choices of $a_z(0) \in [-1, 1]$) and all possible times $t \geq 0$. According to (1) this is formally equivalent to determining the maximum of $\|\rho_b(t) - \rho_f(t)\|_1$ which in this case is given by the function

$$\begin{aligned} \|\rho_b(t) - \rho_f(t)\|_1 = D(t; a_z(0)) := & \left\{ [(e^{-\gamma_f t} - e^{-\gamma_b t})a_z(0) + a_z^{(f)}(\infty)(1 - e^{-\gamma_f t}) - a_z^{(b)}(\infty)(1 - e^{-\gamma_b t})]^2 \right. \\ & \left. + (e^{-\gamma_f t/2} - e^{-\gamma_b t/2})^2 (1 - a_z^2(0)) \right\}^{1/2}. \end{aligned} \quad (28)$$

The best way to approach the problem seems to first optimize with respect to $a_z(0)$ and then maximize with respect to t . We call $(\bar{t}, \bar{a}_z(0))$ the point where the maximum value of $D^2(t; a_z(0))$ is attained.

Let us fix t and rewrite $D^2(t; a_z(0))$ as a parabola in $a_z(0)$:

$$D^2(t; a_z(0)) = f_-^2 (f_+^2 - 1) a_z^2(0) + 2A f_- f_+ a_z(0) + f_-^2 + A^2, \quad (29)$$

with

$$f_{\pm} := e^{-\frac{\gamma_t}{2}} \pm e^{-\frac{\gamma_t}{2y}}, \quad A := -x(1 - e^{-\gamma t}) + y(1 - e^{-\frac{\gamma t}{y}}), \quad (30)$$

where we used (18) to express the dependence upon β_b and β_f . Since $a_z(0) \in [-1, 1]$, $\bar{a}_z(0)$ is either one of the extrema -1 and 1 or the abscissa of the vertex $V = Af_+/[f_-(1 - f_+^2)]$ of the parabola (29). The condition for the vertex to be the maximum is that the parabola is concave down and that the abscissa of the vertex falls strictly inside the interval $] -1, 1[$:

$$\frac{f_-}{f_+} (1 - f_+^2) > |A| \Leftrightarrow \bar{a}_z(0) = V \in] -1, 1[. \quad (31)$$

On the other hand, its violation imposes that the maximum is one of the extrema depending on the sign of A

$$\frac{f_-}{f_+} (1 - f_+^2) \leq |A| \Leftrightarrow \bar{a}_z(0) = \text{sign}[A]. \quad (32)$$

The equation above holds for $A \neq 0$, when $A = 0$ the points $a_z(0) = 1$ and $a_z(0) = -1$ are two equivalent maxima (still provided that the function is concave up).

Eventually, we have to find the maximum among $D^2(t_1; V_{t_1})$, $D^2(t_2; 1)$, $D^2(t_2; -1)$ for all t_1 satisfying inequality (31) and t_2 satisfying inequality (32). The explicit values of the three quantities above can be computed from Eq. (29) and read:

$$D^2(t_1; V_{t_1}) = \frac{f_-^2(t_1)(f_+^2(t_1) - 1) - A^2(t_1)}{f_+^2(t_1) - 1}; \quad (33)$$

$$D^2(t_2; 1) = (f_+(t_2)f_-(t_2) + A(t_2))^2; \quad (34)$$

$$D^2(t_2; -1) = (f_+(t_2)f_-(t_2) - A(t_2))^2. \quad (35)$$

Such maximization procedure yields the point $(\bar{t}, \bar{a}_z(0))$ we were searching for fixed x and y . However, notice that in general (for both the cases in which the concavity is up and down) the sign of A determines the sign of $\bar{a}_z(0)$

$$\text{sign}[\bar{a}_z(0)] = \text{sign}[A], \quad (36)$$

implying that in the region

$$y \geq x \Rightarrow \bar{a}_z(0) > 0. \quad (37)$$

Moreover, condition (31) cannot be satisfied for t sufficiently close to 0 such that

$$\frac{\gamma t/2}{\log\left(\frac{1}{1-\exp(-\gamma t/2)}\right)} \leq y \Rightarrow \bar{a}_z(0) = \text{sign}[A]. \quad (38)$$

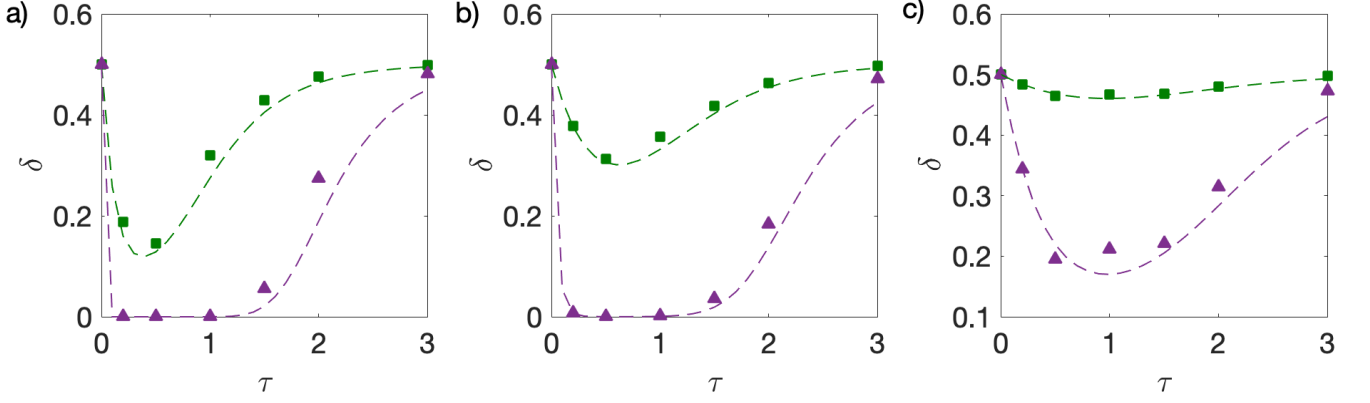


FIG. 5. Estimation errors for statistical tagging. The error δ is reported for a) $\beta_b = \beta_f = 0.5$ b) $\beta_b = \beta_f = 1$ c) $\beta_b = \beta_f = 2$ ($\omega \equiv 1$). In all panels, points are evaluations of the expected errors based on the experimental probabilities, and the curves are the ideal cases for $N = 10$ (green squares) or $N = 100$ (purple triangles). The probe was initialized in the excited state.

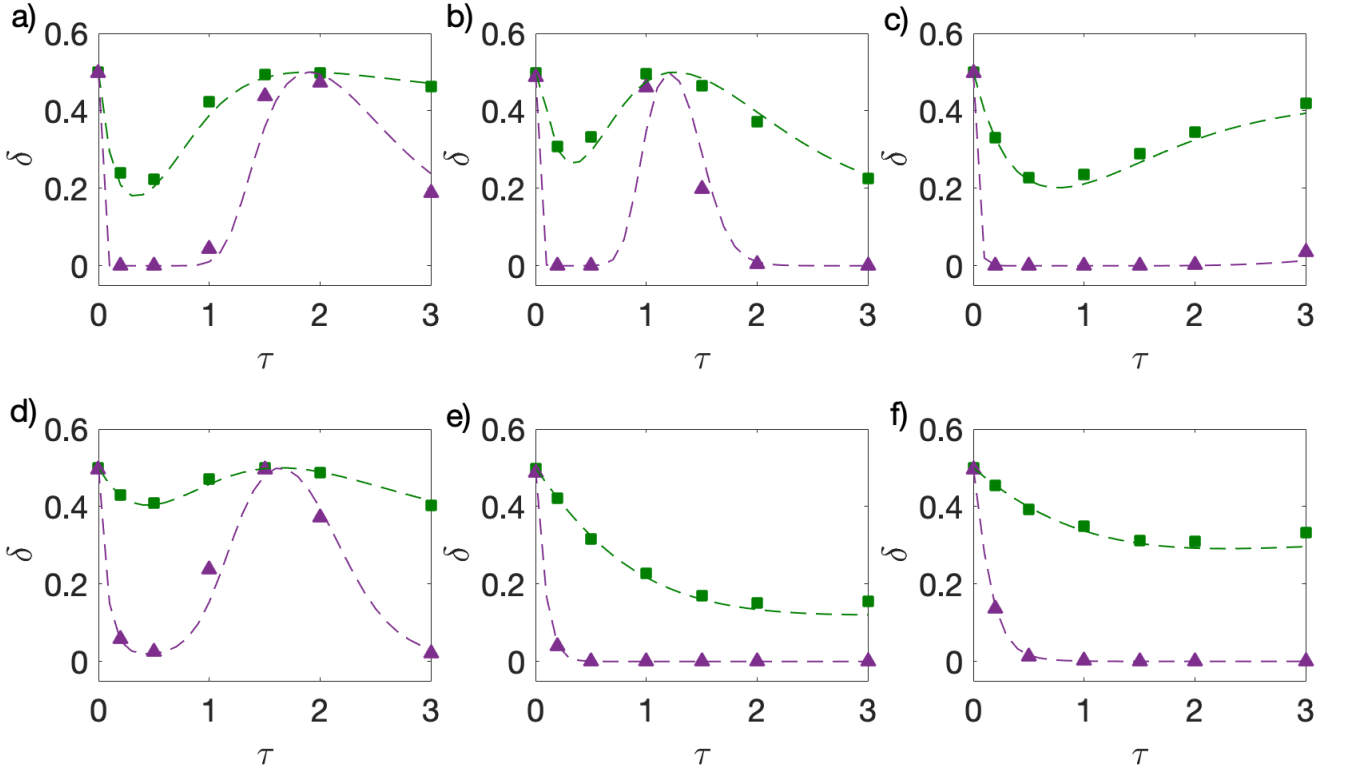


FIG. 6. Estimation errors for general bath discrimination. The error δ is reported for a) $\beta_b = 0.5, \beta_f = 1$ b) $\beta_b = 0.5, \beta_f = 2$ c) $\beta_b = 1, \beta_f = 0.5$ d) $\beta_b = 1, \beta_f = 2$ e) $\beta_b = 2, \beta_f = 0.5$ f) $\beta_b = 2, \beta_f = 1$ ($\omega \equiv 1$). In all panels, points are evaluations of the expected errors based on the experimental probabilities, and the curves are the ideal cases for $N = 10$ (green squares) or $N = 100$ (purple triangles). The probe was initialized in the excited state.

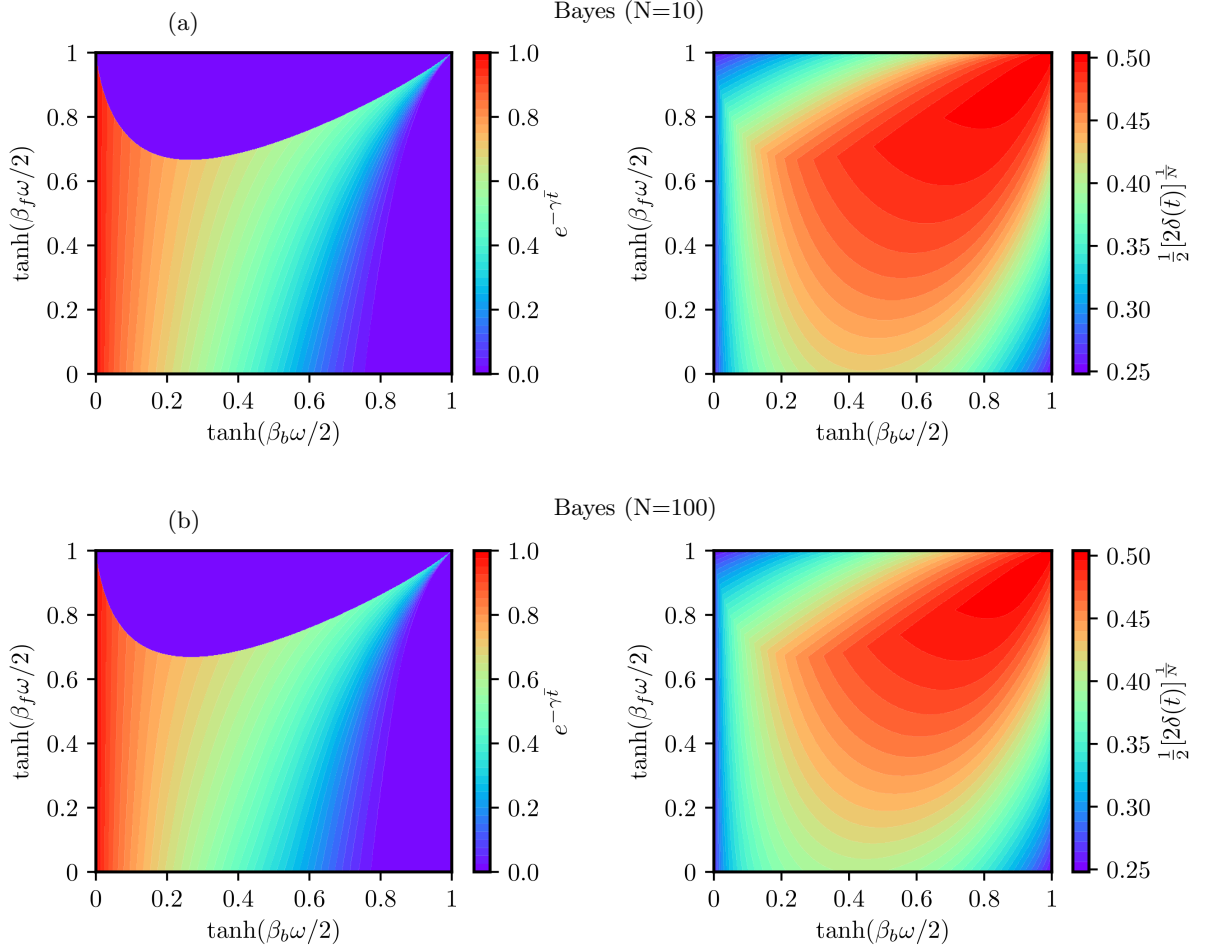


FIG. 7. Same study as in Fig. 1 but for the error probability δ of Eq. (16) based on the Bayesian approach for $N=10$ (Panel a) and $N=100$ (Panel b). To allow a direct comparison for different N and with the figures of merit of Fig. 1, we report instead of δ its rescaled version $1/2[2\delta]^{1/N}$. We remark that as for Fig. 1 the probe was initialized in the excited state.

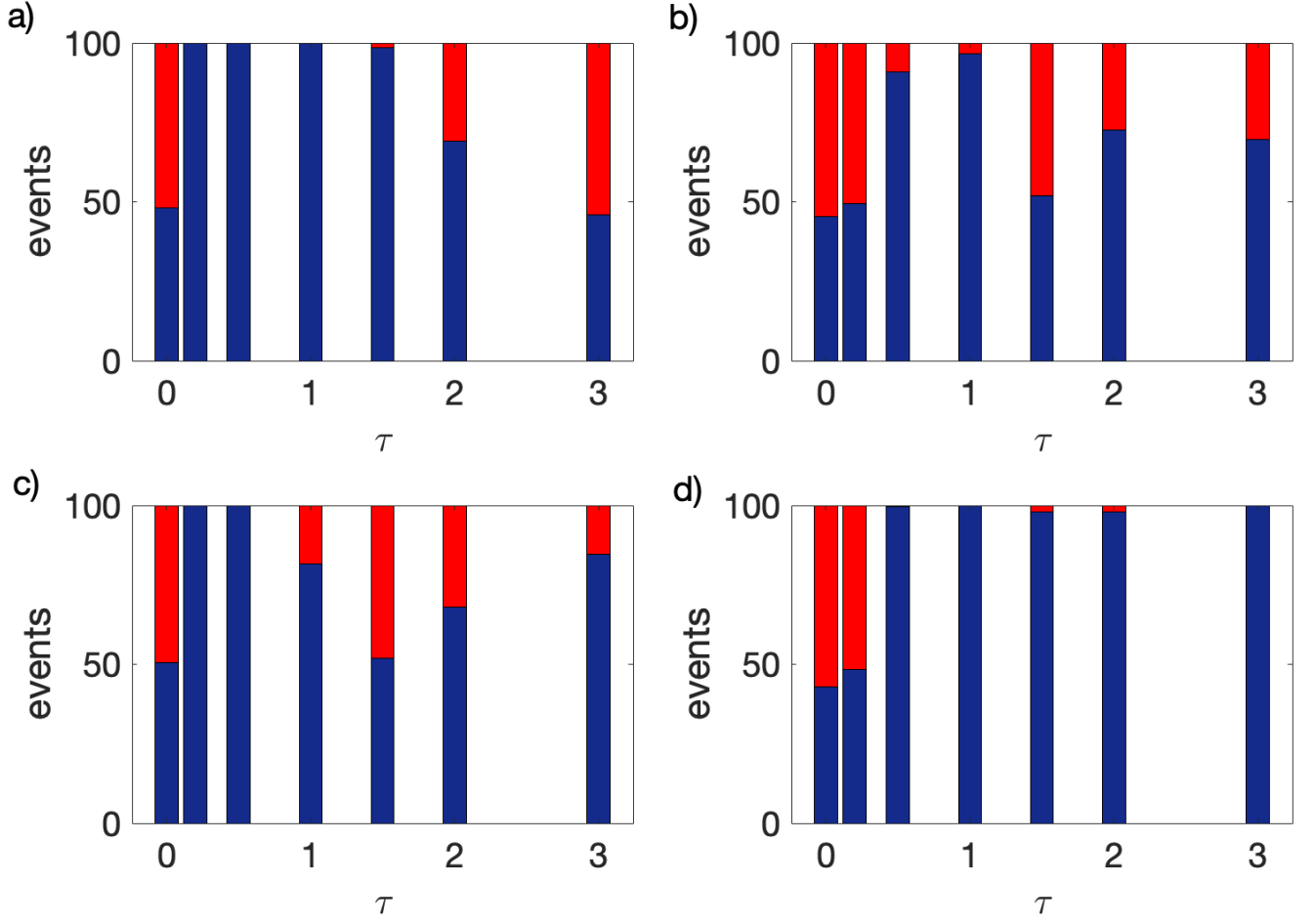


FIG. 8. Bayesian bath discrimination. The histogram report the events correctly identified in blue (lower part of the histogram bars), and the incorrect ones in red (upper part of the bar). The discrimination tasks are a) statistical tagging with $\beta_b = \beta_f = 0.5$, b) statistical tagging with $\beta_b = \beta_f = 2$, c) bath discrimination with $\beta_b = 0.5, \beta_f = 1$, c) bath discrimination with $\beta_b = 2, \beta_f = 1$ ($\omega \equiv 1$). The probe was initialized in the excited state.